The nature of the di-iron site in the bacterio-ferritin from *Desulfovibrio desulfuricans*

Sofia Macedo[1,2], Célia V. Romão[1], Edward Mitchell[2], Pedro M. Matias[1], Ming Y. Liu [3], António V. Xavier[1], Jean LeGall[3], Miguel Teixeira[1], Peter Lindley[1,2] and Maria A. Carrondo[1]

Published online 10 March 2003; doi:10.1038/nsb909

The first crystal structure of a native di-iron center in an iron-storage protein (bacterio)ferritin is reported. The protein, isolated from the anaerobic bacterium *Desulfovibrio desulfuricans,* has the unique property of having Fe-coproporphyrin III as its heme cofactor. The three-dimensional structure of this bacterioferritin was determined in three distinct catalytic/redox states by X-ray crystallography (at 1.95, 2.05 and 2.35 Å resolution), corresponding to different intermediates of the di-iron ferroxidase site. Conformational changes associated with these intermediates support the idea of a route for iron entry into the protein shell through a pore that passes through the di-iron center. Molecular surface and electrostatic potential calculations also suggest the presence of another ion channel, distant from the channels at the three- and four-fold axes proposed as points of entry for the iron atoms.

© 2003 Nature Publishing Group http://www.nature.com/naturestructuralbiology

Ferritins are ubiquitous iron storage proteins present in most forms of life that, together with iron-transporting proteins, enable a tight regulation of the iron concentration in living cells[1]. The storage of iron (up to ~4,500 atoms per holoprotein) allows the cells to have a continuous supply of this essential metal, compensating for its low solubility in aqueous media at physiological pH and, at the same time, avoiding the deleterious effects that result from the reactivity of free iron ions with oxygen and oxygen-reactive species.

The structures of the iron-storage ferritin proteins are conserved and generally constituted by a spherical shell composed of 24 protein subunits with two-, three- and four-fold molecular symmetry axes; the monomer is a four α-helix bundle[2]. In 1978, horse spleen ferritin became the first ferritin for which a three-dimensional structure was determined[3]. This protein plays a key role in the oxidation of external ferrous iron to ferric iron, which is then stored inside the large internal protein cavity in a mineral form. Ferritins isolated from bacteria may also contain a heme b group and are then named bacterioferritins (Bfr). This heme is located between two subunits that form the dimer, with a methionine from each monomer providing an axial ligand to the heme iron. The Bfr from the anaerobic sulfate/nitrate reducer *Desulfovibrio desulfuricans* ATCC 27774 (*Dd*) has a di-iron–occupied ferroxidase center in its native form. EPR studies are consistent with this center being in the diferric state in the 'as-isolated' form of the protein — that is, when the protein is anaerobically purified and exposed to air[4]. Furthermore, in contrast to all other isolated Bfrs, *Dd* Bfr has the unique feature of having Fe-coproporphyrin III as its heme cofactor, the first example of this type of heme in a biological system[5]. The physiological electron donor of this Bfr has been identified as a type-II rubredoxin; the genes encoding both the *Dd* Bfr and its electron donor form a dicistronic transcriptional unit[6].

Several ferritin[7–11] and bacterioferritin[12] crystallographic structures have been refined to a resolution of 2.0 Å or higher.

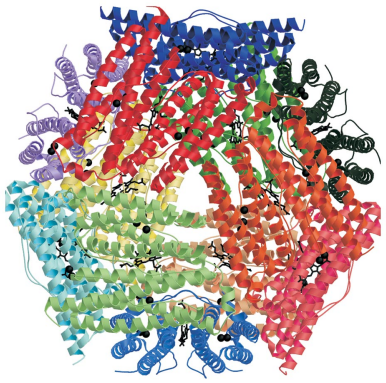

Fig. 1 Overall view of the *Dd* Bfr in structure A. The different colors represent the 12 dimers; the di-iron centers and the heme cofactors are represented in black.

However, the only ferritins that show the presence of iron in their structures are those of the dodecameric ferritin from *Listeria innocua*[13] and *Escherichia coli* (*Ec*) ferritin[11]. In the first case, one single iron atom was located at the interface between monomers, whereas in the second, three iron atoms per monomer (two forming a di-iron site) were inserted in the crystals by soaking in a ferrous salt solution. In bacterioferritin structures, the di-metal site is either filled with two Mn^{2+} ions from the crystallization mother liquor (*Ec* Bfr)[12,14,15] or has low iron occupation as in *Rhodobacter capsulatus* (*Rc*) Bfr[16].

The isolation of *Dd* Bfr with a di-iron center prompted its study by X-ray crystallography in several catalytic/redox states. Crystallization and phase determination of the *Dd* Bfr structure, from crystals of an as-isolated protein sample, have been reported[17]. The MAD measurements at and near the iron K-edge allowed unequivocal identification of the iron atomic positions forming the ferroxidase site and at the center of the

[1]Instituto de Tecnologia Química e Biológica, Universidade Nova de Lisboa, Av. República, EAN, Apartado 127, 2781-901 Oeiras, Portugal. [2]ESRF, BP-220, F-38043 Grenoble Cedex, France. [3]Department of Biochemistry, University of Georgia, Athens, Georgia 30602, USA.

Correspondence should be addressed to M.A.C. *e-mail: carrondo@itqb.unl.pt*

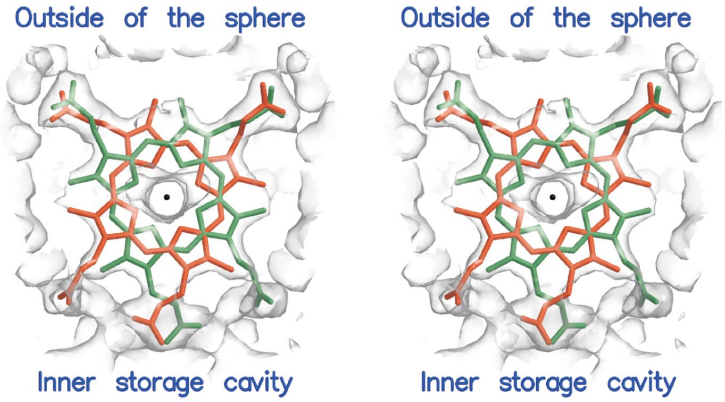

Fig. 2 Stereo view of the electron density averaged over eight independent dimers of the Fe-coproporphyrin III heme cofactor in structure A. The electron density is represented in a 2 $|F_o| - |F_c|$ map contoured at 1.0 σ. The electron density for the Met57 axial ligands is visible above and below the heme group but, for reasons of clarity, these residues were not represented. The geometrical disorder of the heme group in all three structures is similar, and the occupancies for each conformer are ~0.5. Different colors (red and green) represent the two modeled conformations (I and II, respectively), which are related by the noncrystallographic two-fold axis of the Bfr homodimer.

© 2003 Nature Publishing Group http://www.nature.com/naturestructuralbiology

Fe-coproporphyrin III group. Here we present three different structures of *Dd* Bfr: structure A, to 1.95 Å resolution from an as-isolated protein sample; structure B, at 2.05 Å resolution from a sample prepared and crystallized as for structure A and then followed by reduction of the crystal; and structure C, to 2.35 Å resolution from a 'cycled' oxidized sample (see Methods).

Overall structure and topology

Similarly to all the ferritins described structurally so far[18], *Dd* Bfr is an oligomer of 24 monomer subunits that assembles to form a sphere with 432 symmetry. In the crystal structure, the asymmetric unit comprises one-third of two independent molecules — that is, a total of 16 monomers, equivalent to 2 × 4 dimers. Each dimer has an Fe-coproporphyrin III heme between the two monomers in the dimer (eight hemes per asymmetric unit), and each monomer has a native di-iron center (a total of 16 di-iron centers per asymmetric unit) (Fig. 1). The sphere has an external diameter of ~130 Å and an internal cavity for iron storage with a diameter of ~85 Å. Each of the monomers is built up of a four–α-helix bundle containing the di-iron site, with a final fifth shorter helix at the C terminus arranged transversally across the bundle axis (Fig. 1). The hydrophilic channels on the three-fold axes of the molecule are formed by alternating positively and negatively charged residues. Thus, Lys111 and Glu115 define the outer entrance to the channel, and the inner surface is lined by Lys114, Glu126 and Arg123. The uncharged channels on the four-fold axes are lined by four symmetry-related threonines, Thr152.

Heme site

The Fe-coproporphyrin III groups are located on the noncrystallographic two-fold axis of each Bfr homodimer at the interface between monomers. The hemes were refined with two possible conformations (I and II, Fig. 2), a situation similar to that observed in *Rc* Bfr[16]. The hemes are axially coordinated by the Met57 from noncrystallographic symmetry-related monomers and are further linked to the polypeptide chain through hydrogen bonds between propionates A and D to Arg20 and Tyr35, propionate B to Lys50 and propionate C to Ser168; there are more interactions with the polypeptide chain than in heme b–containing ferritins. Residue Arg20, which stabilizes one of the two extra propionates of *Dd* Bfr iron-coproporphyrin, is substituted by nonpolar residues in all other known Bfr sequences, with the exception of two other *Desulfovibrio* species (*D. vulgaris* Hildenborough and *D. desulfuricans* G 20).

Di-iron site

The residues involved in the coordination of the di-iron sites are Glu23 and His59 as terminal ligands to Fe1, and Glu99 and His135 as terminal ligands to Fe2, and Glu56 and Glu132 as bridging ligands (Fig. 3). The ferroxidase di-iron site is flanked by two tyrosine residues, Tyr30 and Tyr106, which are hydrogen-bonded to the terminal glutamate ligands, Glu99 and Glu23, respectively. The two histidine ligands, His59 and His135, are hydrogen-bonded to carboxylate oxygen atoms of Glu131 and Asp55, located at the internal surface of the sphere. The coordination and spatial arrangement of the ferroxidase center is similar to that observed in *Ec* Bfr and resembles that observed in a variety of di-iron proteins that have functions as diverse as the oxygenation of methane, reduction of ribonucleotides and oxygen reduction or transport[19–22].

A close examination of the electron density maps (Fig. 3*b*,*d*,*f*) of the three states of *Dd* Bfr reveals some important features. The structure of the protein as isolated (A) clearly shows electron density lying continuously over the di-iron site, on the opposite side from the histidyl ligands (Fig. 3*b*). This electron density cannot be modeled unequivocally because it likely results from a mixture of different bridging intermediates in the protein sample. Terminal water oxygens, a peroxo intermediate and/or oxo (hydroxo) bridging ligands can be modeled into the residual electron density with acceptable geometry, but refinement of these models at 1.95 Å resolution was not able to distinguish between the three possibilities. Indeed, the electron density may correspond to a mixture of different intermediates as a result of the reduction of molecular oxygen at the ferroxidase sites in ferritins[11] or bacterioferritins[23,24]. The average value reported in the present study for the iron···iron distance, 3.71 Å in structure A, is typical of di-iron centers found in many other di-iron proteins[22], which can have oxo or water bridging ligands. The bridging electron density is not present in the structure of the reduced crystal (B; Fig. 3*d*). One single terminal water ligand lying at a distance of 2.46 Å from Fe1 is, nevertheless, clearly defined and was therefore included in the final refinement. The longer Fe1···Fe2 average distance of 3.99 Å observed in structure B is compatible with

© 2003 Nature Publishing Group http://www.nature.com/naturestructuralbiology

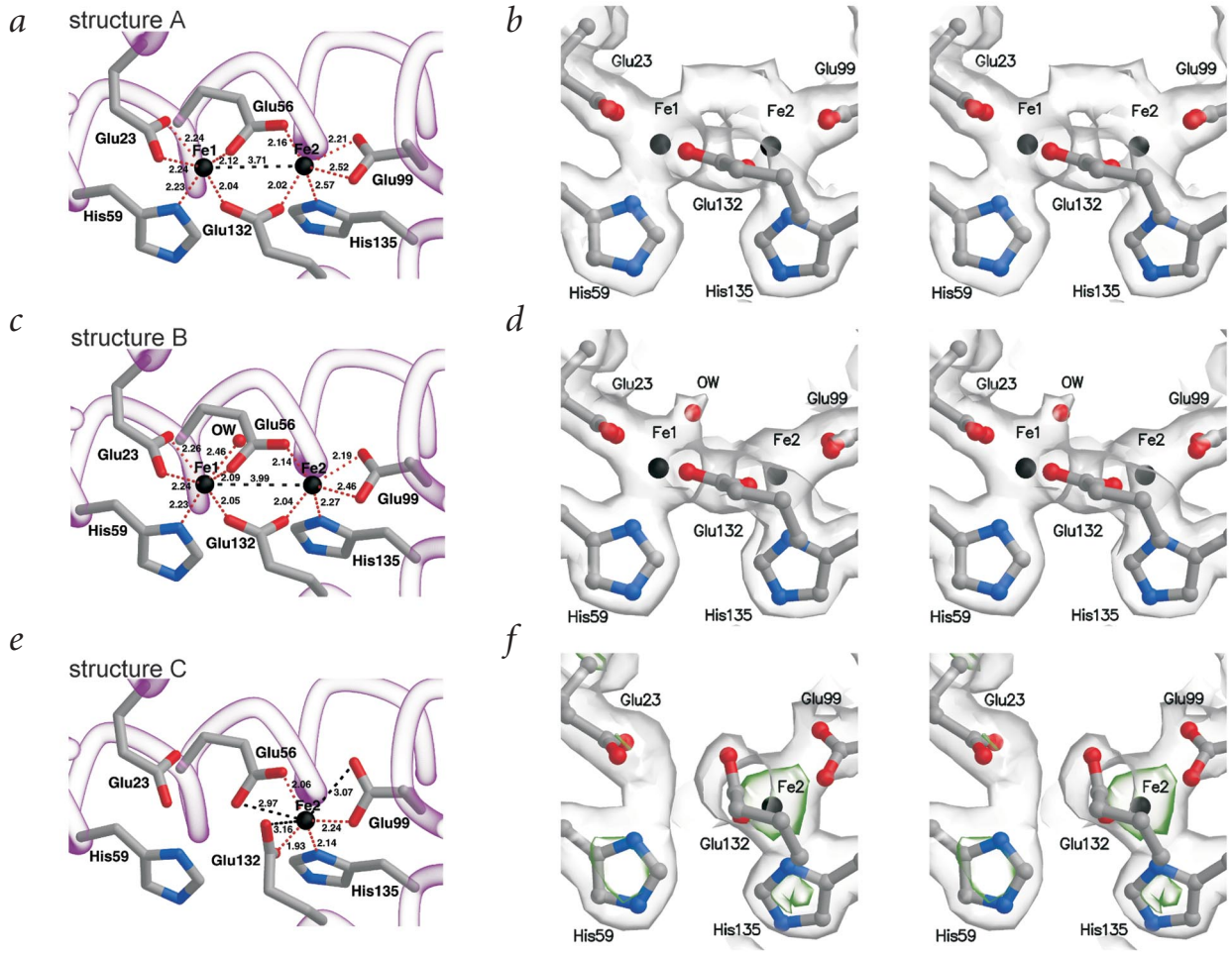

Fig. 3 The di-iron center of *Dd* Bfr. Bond lengths (Å) are always average values for the 16 crystallographically independent monomers. The bridging ligands and their coordination (dashed red lines) and van der Waals distances (dashed black lines) to the iron atoms are shown in the three schemes. ***a***, A schematic view of structure A. ***b***, Stereo view of electron density in a 2 $|F_o| - |F_c|$ map contoured at 1.5 σ in the vicinity of the di-iron center in structure A. The electron density bridging the iron atoms can be interpreted as a mixture of oxygen atoms constitutive of a peroxo/oxo intermediate ligand and terminal waters. ***c***, A schematic view of the structure B. ***d***, Stereo view of stucture B as in (*b*). The bridging electron density is reduced to a single water molecule, OW, bound to Fe1. ***e***, A schematic view of the structure C. ***f***, Stereo view of structure C as in (*b*). The electron density at 5.0 σ (green) shows that Fe1 remains present in the structure with only a low occupancy.

a reduced diferrous state[22]. The bridging ligands in structure A, together with the increase in the iron-to-iron distance in structure B relative to structure A, strongly support the hypothesis that this is an intermediate structure in the ferroxidase reaction, with the iron atoms predominantly in the oxidized state[22]. When the protein sample was reduced fully and subsequently allowed to oxidize in the presence of atmospheric oxygen (structure C), the ferroxidase center appeared with Fe1 mostly depleted. No sign of any bridging/terminal oxygen ligand remained in the electron density maps (Fig. 3*f*), nor could a peak be assigned to an ordered iron ion elsewhere in the structure. Glu56 in structure C approaches Fe2, while the carboxylate group of Glu132 undergoes a rearrangement, rotating by nearly 90° about the Cγ-Cδ bond.

Ferroxidase pore

The di-iron center is located at the bottom of a pore in the Bfr monomer. The entrance to this pore is approximately circular in shape and has a radius of ~1.4 Å. This pore is wider at the bottom, with an approximate elliptical contour shape and axes of ~5.3 Å and 4.7 Å, with the major axis roughly aligned with the Fe1-Fe2 direction. These distances were calculated excluding the contributions of the van der Waals radii of the atoms forming the pocket, but they can be interpreted in terms of the van der Waals dimensions of species (such as Fe ions and water molecules) that may enter and leave the pore. The Fe atoms are located ~6 Å below the pore entrance. The pore is formed mainly by hydrophilic residues arranged in three layers: a top layer, which defines the entrance and includes Met22, His25, Gln98 and Thr102; a middle layer that defines the side walls and is formed by Ala26, Tyr30, Thr102 and Tyr106; and the bottom layer, which consists of the iron atoms and their glutamate ligands (Glu23, 56, 99 and 132). The pore, represented by views of the external molecular surface near the di-iron center in the three structures (Fig. 4*a–c*), is similar to the pores found in the structures of *Ec* Bfr[14] and *Rc* Bfr[16] and those described for the structure of *Ec* ferritin[11]. Such an observation prompts the hypothesis that the entry of iron for reaction at the ferroxidase site can occur through this pore, forming the di-iron site. Upon reaction with oxygen, the iron atoms were subsequently oxidized (structure C). However, we observed the Fe1 position to be significantly depleted (70–100% for the various subunits).

© 2003 Nature Publishing Group http://www.nature.com/naturestructuralbiology

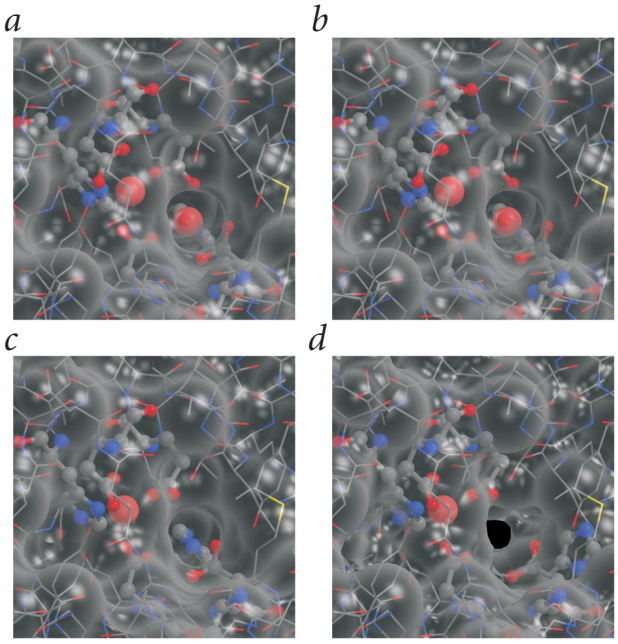

Fig. 4 Views of a Bfr monomer with overlaid molecular surface showing the surface pore that allows access to the di-iron center for structures ***a***, A; ***b***, B; and ***c***, C. ***d***, A hypothetical model of structure C in which His59 and Glu131 have been moved to allow the formation of a second opening in the pore, enabling access to the interior of the Bfr 24-nucleotide oligomer cluster. The molecular surfaces were calculated with MSMS[40] using a probe radius of 1.4 Å in (*a*–*c*) and 0.7 Å in (*d*). Thus, the size of the pore (~1.4 Å radius, see text) is such that Fe ions and water molecules may access it freely. The 0.7 Å probe radius in (*d*) was chosen because it is close to the ionic radius of Fe(III). The interpretation of (*d*) is that if such a histidinyl flip can occur (Phe3 also has to move slightly), the size of the resulting opening allows a sphere with that radius (0.7 Å) to access the inside of the molecular cluster. The iron atoms in the di-iron center are represented as red spheres with an ionic radius of 0.8 Å, and their ligands are drawn as the ball-and-stick models; the rest of the molecule is drawn as bonds-only with thinner lines. A standard coloring scheme — red for O, blue for N, grey for C and yellow for S — has been used to denote the chemical nature of the protein atoms.

Under the conditions in which this reaction was carried out, this Fe atom may have left the di-iron site to the solvent through the pore. Nevertheless, under physiological conditions, this Fe atom may be translocated into the inner core *via* a concerted movement of His59 and Glu131, which would open up a continuous channel to the sphere core (Fig. 4*d*). These residues can change conformation, perhaps induced by local pH variations, avoiding clashes with neighboring residues during this process.

In the case of the *Ec* ferritin[11], two iron ions formed the di-iron site and a third ion penetrated as far as the inner surface of the protein. The coordination of this third iron was accomplished, by comparison with the structure of the apo protein, with the help of a large movement of His46, a residue close to the di-iron site, and a small adjustment of Glu49, a residue close to His46 and at the inner surface of the protein core. Thus, the observed movement of these two residues in *Ec* ferritin[11] and the similar movement proposed here for His59 and Glu131 in *Dd* Bfr may constitute a gating mechanism for the passage of iron from the di-iron site to the inner core.

Electrostatic potential surfaces

An examination of both the internal and the external molecular surfaces of the intact 24-subunit oligomeric protein in *Dd* Bfr (structure A) reveals a preponderance of negatively charged residues, which is emphasized by the electrostatic potentials of these surfaces (Fig. 5). This distribution of negative charges (–132 overall in *Dd* Bfr, assuming +3 for iron atoms) has been reported in other ferritins[18,25]. In *Dd* Bfr, iron access through the three-fold and four-fold channels is unlikely because of the alternating distribution of positively and negatively charged residues along those channels. However, on the outside surfaces of *Dd* Bfr, there are clusters of negative charges at channels located between the three-fold and four-fold axes (designated B, Fig. 5). These channels are sufficiently large enough to admit the entry of iron atoms and provide a route of access to the core of the protein. In *Dd* Bfr structure A, the electrostatic potential at the ferroxidase center is dominated by the positive charges of the iron atoms. However, in structure C, the positive charge of the single iron atom is insufficient to compensate for the negative charges of the neighboring glutamic acid residues, and the electrostatic potential at the ferroxidase center becomes negative

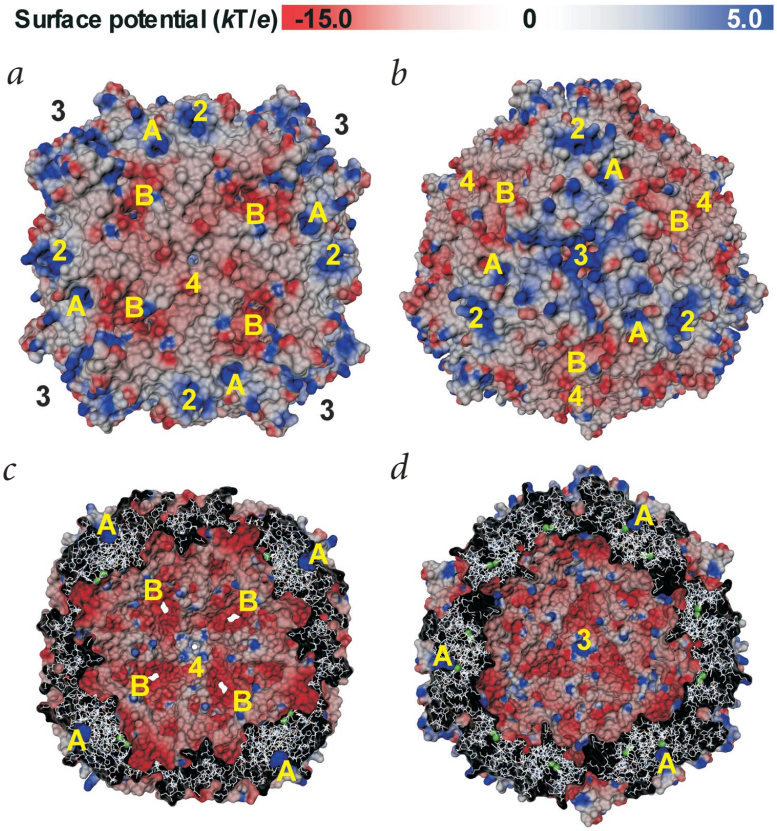

Fig. 5 Electrostatic potential surfaces of *Dd* Bfr. ***a***, External surface view down a noncrystallographic four-fold axis. ***b***, External surface view down a crystallographic three-fold axis. ***c***, Internal surface view up a noncrystallographic four-fold axis. ***d***, Internal surface view up a crystallographic three-fold axis. 'A' represents the ferroxidase pore; 'B', major channel; '2', two-fold noncrystallographic axis; '3', three-fold crystallographic axis; and '4', four-fold noncrystallographic axis. The ferroxidase iron atoms are represented as green spheres. The molecular surfaces were calculated with MSMS[40] using a probe radius of 1.4 Å. The electrostatic potentials were calculated with MEAD[41] using a protein and external dielectric constants of 4 and 80, respectively, a temperature of 300 K and an ionic strength of 0.1 M.

© 2003 Nature Publishing Group http://www.nature.com/naturestructuralbiology

Table 1 Data collection, processing and structure refinement statistics for *Dd* Bfr

	Structure A	Structure B	Structure C
Data collection			
Resolution (Å)	30–1.95	30–2.05	30–2.35
Space group	$P2_13$	$P2_13$	$P2_13$
Cell edge (Å)	225.3	225.7	225.8
Observations	905,598	871,754	477,229
Unique reflections	271,259	234,647	152,336
Redundancy[1]	3.3 (3.1)	3.7 (3.6)	3.1 (3.1)
Completeness (%)[1]	98.9 (97.6)	99.0 (99.8)	96.5 (99.0)
R_{merge} (%)[1,2]	6.6 (34.3)	5.7 (29.9)	6.2 (21.6)
$I / \sigma (I)$ [1]	6.4 (2.1)	8.1 (2.4)	6.8 (2.7)
Wilson *B*-factor (Å^2)	28	29	35
Refinement statistics			
R_{cryst} (%)[3]	21.4	23.1	19.7
R_{free} (%)[4,5]	25.4 (0.015)	27.0 (0.021)	26.7 (0.020)
R.m.s. deviations from standard geometry (Å)			
1,2 bond distances	0.011	0.006	0.004
1,3 bond (angle) distances	0.025	0.018	0.015

[1]Numbers in parentheses refer to the highest resolution shell: 2.02–1.95 Å; 2.12–2.05 Å and 2.43–2.35 Å for structures A, B and C, respectively.
[2]$R_{merge} = \Sigma| I_o - <I>| / \Sigma I_o$.
[3]$R_{cryst} = \Sigma||F_o| - |F_c|| / \Sigma|F_o|$.
[4]$R_{free} = R_{cryst}$ calculated for reflections not included in the refinement. Because of the high NCS within the asymmetric unit, and to minimize bias, reflections for R_{free} were chosen randomly in thin resolution shells.
[5]Number in parentheses is the fraction of total reflections.

(data not shown). This may be one of the driving forces leading to the reconstitution of the ferroxidase center: uptake of ferrous ions from the surroundings.

On the basis of amino acid sequence comparisons, the three- and four-fold axes channels described for the mammalian proteins have been suggested to be inoperative in the bacterial ferritins[2,11]. An examination of the electrostatic potential surfaces of *Ec* Bfr (PDB entry 1BCF), *Ec* ferritin (1EUM), horse spleen ferritin (1IER) and human H-chain ferritin (2FHA) shows that the B channels shows that the B channels (Fig. 5) seem to be unique to the bacterial proteins, unless they occur in mammalian ferritins through conformational changes of surface residues.

Final considerations

It is commonly accepted that the first step of iron uptake by (bacterio)ferritins is the build-up of the di-iron center upon addition of ferrous iron to the apo protein. However, at least for the *Dd* Bfr, the protein is isolated with a complete di-iron site, suggesting that this center is intrinsically attached to the protein *in vivo*, possibly leading to a different mechanism of iron oxidation and storage.

Recently, a mechanism was proposed for the oxidation of iron in *Ec* Bfr that assumed hydrogen peroxide was an intermediate product resulting from the reduction of molecular oxygen at the ferroxidase center[23,24]. A complete reduction to water was also observed. The electron density observed for the as-isolated protein in the di-iron site was not as clearly interpretable in terms of a single ligand species to the iron atoms. This electron density may result from a combination of different stages of the ferroxidase reaction with oxo or peroxo bridges as it occurs in the bacterioferritin 24-subunit oligomeric protein, averaged over the entire crystal structure. As the protein was isolated anaerobically but crystallized aerobically, the oxidant leading to the intermediates now observed and described above was molecular oxygen. The role of iron storage proteins and the physiological oxidant for the ferroxidase step remains to be established in anaerobic bacteria. Because of the close association between the iron and oxygen metabolisms, (bacterio)ferritins may be important in the oxidative stress response of anaerobes upon transient exposure to oxygen or oxygen reactive species, which involves scavenging iron inside the protein and avoiding the production of the highly deleterious oxygen radical species formed under those conditions in the presence of free iron ions.

After reduction followed by reaction with oxygen, only one of the iron atoms detaches from the di-iron site, possibly finding its way into the protein cavity. Restoration of the ferroxidase center may occur upon arrival of a new iron ion through the pore that extends from the external protein surface to the di-iron site. Such an entry mechanism could be far more specific to iron compared with other metals. After formation of the initial nucleation sites inside the protein core, iron may enter directly into the core through the B-type channels (Fig. 5), which are distinct from the channels at the three- or four-fold axes, and may be subsequently oxidized in the core during the latest stages of mineralization[26].

Methods

Crystallization. The crystals used in these structural studies were prepared as described[17]. For structure A the protein was purified anaerobically in a partially reduced state, as indicated by the heme visible spectra, and was crystallized aerobically. However, visible spectra of these crystals showed that the crystallized protein has the heme center in the oxidized state. For structure B, the sample was prepared and crystallized as for structure A, and crystals were reduced by soaking in excess sodium dithionite before cryo-protection and flash freezing. For structure C, the protein solution was fully reduced, excess dithionite was removed by gel filtration and the protein was allowed to re-oxidize by exposure to oxygen, followed by aerobic crystallization. The electronic spectrum of this preparation showed that the heme center was fully oxidized. The cryo-protectant solutions for the three crystals were obtained by preparing a crystallization solution[17] containing 25% (v/v) glycerol.

X-ray data collection and processing. Diffraction data were collected using X-ray wavelengths of 0.933 Å at ESRF beamline ID14-2 on an ADSC Q4 CCD detector to 1.95 Å, 2.05 Å and 2.35 Å resolution (structure A, B and C, respectively). All diffraction images were integrated using the HKL suite[27] and subsequently scaled together, reduced and truncated using the CCP4 suite[28]. Data collection and processing statistics are shown in Table 1.

Model building and refinement. For structure A, the initial phasing information was obtained from a MAD experiment at the iron K-edge, as described[17]. Phases to 2.8 Å resolution, obtained from this MAD experiment, were extended to 1.95 Å by a density modification procedure with DM[29]. The resulting electron density map was of excellent quality and was used to trace the Cα chain of a single dimer using O[30]. This Cα trace of the dimer was then used together with the iron atom positions located from the MAD data to manually find and subsequently improve, using IMP[31] and DM, the eight noncrystallographic symmetry matrices necessary to construct the complete asymmetric unit. Most of the remaining structure was then built using O[30], but the di-iron sites and heme cofactors were added only at a later stage. The Fe-coproporphyrin III heme cofactor[5] was modeled in two different conformations. Water molecules were added based on SigmaA[32]-weighted $|F_o| - |F_c|$ difference Fourier map density of at least 3 σ and sensible hydrogen bonding

patterns. Model refinement with CNS[33], REFMAC[34] and in the last cycles with SHELXL[35] gave a final model with 2,717 residues (out of a possible 2,864), 1,890 water molecules, 40 iron atoms, 25 glycerol molecules and 52 sulfate ions.

For structures B and C, the final model of structure A, excluding water molecules, the di-iron sites and the heme groups, was used as a starting point for the refinement. Simulated annealing with CNS[33] was used to reduce model bias. The same refinement strategy as for structure A resulted in a final model for structure B with 2,711 residues (out of a possible 2,864), 1,659 water molecules, 40 iron atoms, 0 glycerol molecules and 55 sulfate ions. Likewise, the final model for structure C comprised 2,716 residues, 1,811 water molecules, 24 iron atoms, 1 glycerol molecule and 33 sulfate ions. Model statistics are given in Table 1.

The refinement of the asymmetric unit for the three redox states A, B and C gave similar overall structures. The average Cα r.m.s. deviation (calculated with O[30] for 2,704 Cα atoms) is 0.38 Å, 0.24 Å and 0.37 Å after superposition of A and B structures, B and C structures, and A and C structures, respectively. The structures were analyzed with PROCHECK[36] and the stereochemical quality parameters are within their respective confidence intervals. The Ramachandran plots of the three structures revealed that 96.9%, 95.7% and 95.9% (for structures A, B and C, respectively) of non-glycine and non-proline residues are within the allowed regions. The *Dd* Bfr overall structures are also highly similar to the *Ec* Bfr[15] and the *Rc* Bfr[16] structures (r.m.s. deviations in Cα positions of 1.25 Å and 1.61 Å, respectively, to structure A).

Figs. 1, 4 were prepared with MolScript[37] and Raster3D[38]. Fig. 2 was prepared with BobScript[39] and Raster3D. Fig. 3 was prepared with MolScript, BobScript and Raster3D. Fig. 5 was prepared with DINO (*http://www.dino3d.org*).

Coordinates. Structure factors for the three data sets and associated structure coordinates were deposited in the Protein Data Bank (accession codes 1NFV (structure A), 1NF4 (structure B) and 1NF6 (structure C)).

Acknowledgments

This work was supported by PRAXIS XXI and POCTI grants. We thank the ESRF, Grenoble (France) for the provision of synchrotron radiation and for a grant to S.M.

Competing interests statement

The authors declare that they have no competing financial interests.

Received 23 October, 2002; accepted 3 February, 2003.

1. Crichton, R. Intracellular iron storage and biomineralization. in *Inorganic Biochemistry of Iron Metabolism: From Molecular Mechanisms to Clinical Consequences* 2nd edn. (eds. Boelaert, J.R. *et al.*) 133–165 (John Wiley, Chichester; 2001).
2. Harrison, P.M., Hempstead, P.D., Artymiuk, P.J. & Andrews, S.C. Structure-function relationships in the ferritins. in *Metal Ions in Biological Systems* Vol. 35 (eds. Siegel, A. & Siegel, H.) 435–477 (Marcel Dekker, New York; 1998).
3. Banyard, S.H., Stammers, D.K. & Harrison, P.M. Electron density map of apoferritin at 2.8-Å resolution. *Nature* **271**, 282–284 (1978).
4. Romão, C.V. *et al.* A bacterioferritin from the strict anaerobe *Desulfovibrio desulfuricans* ATCC 27774. *Biochemistry* **39**, 6841–6849 (2000).
5. Romão, C.V. *et al.* Iron-coproporphyrin III is a natural cofactor in bacterioferritin from the anaerobic bacterium *Desulfovibrio desulfuricans*. *FEBS Lett.* **480**, 213–216 (2000).
6. da Costa, P.N. *et al.* The genetic organization of *Desulfovibrio desulphuricans* ATCC 27774 bacterioferritin and rubredoxin-2 genes: involvement of rubredoxin in iron metabolism. *Mol. Microbiol.* **41**, 217–227 (2001).
7. Trikha, J., Theil, E.C. & Allewell, N.M. High resolution crystal structures of amphibian red-cell L ferritin: potential roles for structural plasticity and solvation in function. *J. Mol. Biol.* **248**, 949–967 (1995).
8. Gallois, B. *et al.* X-ray structure of recombinant horse L chain apoferritin at 2.0 Å resolution: implications for stability and function. *J. Biol. Inorg. Chem.* **2**, 360–367 (1997).
9. Hempstead, P.D. *et al.* Comparison of the three-dimensional structures of recombinant human H and horse L ferritins at high resolution. *J. Mol. Biol.* **268**, 424–448 (1997).
10. Granier, T. *et al.* Structure of mouse L-chain ferritin at 1.6 Å resolution. *Acta Crystallogr. D* **57**, 1491–1497 (2001).
11. Stillman, T.J. *et al.* The high-resolution X-ray crystallographic structure of the ferritin (EcFtnA) of *Escherichia coli*; comparison with human H ferritin (HuHF) and the structures of the Fe^{3+} and Zn^{2+} derivatives. *J. Mol. Biol.* **307**, 587–603 (2001).
12. Frolow, F. & Kalb (Gilboa), A.J. Cytochrome b_1 – bacterioferritin. in *Handbook of Metalloproteins* Vol. 2 (eds. Messerschmidt, A., Huber, R., Poulos, T. & Wieghardt, K.) 782–790 (Wiley, UK; 2001).
13. Ilari, A., Stefanini, S., Chiancone, E. & Tsernoglou, D. The dodecameric ferritin from *Listeria innocua* contains a novel intersubunit iron-binding site. *Nat. Struct. Biol.* **7**, 38–43 (2000).
14. Frolow, F., Kalb (Gilboa), A.J. & Yariv, J. Structure of a unique two-fold symmetric heme-binding site. *Nat. Struct. Biol.* **1**, 453–460 (1994).
15. Dautant, A. *et al.* Structure of a monoclinic crystal from of cyctochrome b_1 (bacterioferritin) from *E. coli*. *Acta Crystallogr. D* **54**, 16–24 (1998).
16. Cobessi, D. *et al.* The 2.6 Å resolution structure of *Rhodobacter capsulatus* bacterioferritin with metal-free dinuclear site and heme iron in a crystallographic 'special position'. *Acta Crystallogr. D* **58**, 29–38 (2002).
17. Coelho, A.V. *et al.* Structure determination of bacterioferritin from *Desulfovibrio desulfuricans* by the MAD method at the Fe K-edge. *Acta Crystallogr. D* **57**, 326–329 (2001).
18. Theil, E.C. Ferritin. in *Handbook of Metalloproteins* Vol. 2 (eds. Messerschmidt, A., Huber, R., Poulos, T. & Wieghardt, K.) 771–781 (Wiley,UK; 2001).
19. Rosenzweig, A.C. *et al.* Crystal structures of the methane monooxygenase hydroxylase from *Methylococcus capsulatus* (Bath): implications for substrate gating and component interactions. *Proteins* **29**, 141–152 (1997).
20. Tong, W. *et al.* Characterization of Y122F R2 of *Escherichia coli* ribonucleotide reductase by time-resolved physical biochemical methods and X-ray crystallography. *Biochemistry* **37**, 5840–5848 (1998).
21. Gomes, C.M., Gall, J.L., Xavier, A.V. & Teixeira, M. Could a diiron-containing four-helix-bundle protein have been a primitive oxygen reductase? *Chembiochem* **2**, 583–587 (2001).
22. Kurtz, D.M. Jr. Structural similarity and functional diversity in diiron-oxo proteins. *J. Biol. Inorg. Chem.* **2**, 159–167 (1997).
23. Yang, X. *et al.* The iron oxidation and hydrolysis chemistry of *Escherichia coli* bacterioferritin. *Biochemistry* **39**, 4915–4923 (2000).
24. Bou-Abdallah, F. *et al.* Iron detoxification properties of *Escherichia coli* bacterioferritin. Attenuation of oxyradical chemistry. *J. Biol. Chem.* **277**, 37064–37069 (2002).
25. Douglas, T. & Ripoll, D.R. Calculated electrostatic gradients in recombinant human H-chain ferritin. *Protein Sci.* **7**, 1083–1091 (1998).
26. Chasteen, N.D. & Harrison, P.M. Mineralization in ferritin: an efficient means of iron storage. *J. Struct. Biol.* **126**, 182–194 (1999).
27. Otwinowski, Z. & Minor, W. Processing of X-ray diffraction data collected in oscillation mode. *Methods Enzymol.* **276**, 307–326 (1997).
28. Collaborative Computational Project, Number 4. The CCP4 suite: programs for protein crystallography. *Acta Crystallogr. D* **50**, 760–763 (1994).
29. Cowtan, K.D. & Main, P. Miscellaneous algorithms for density modification. *Acta Crystallogr. D* **54**, 487–493 (1998).
30. Jones, T.A., Zou, J.Y., Cowan, S.W. & Kjeldgaard, M. Improved methods for building protein models in electron density maps and the location of errors in these models. *Acta Crystallogr. A* **47**, 110–119 (1991).
31. Kleywegt, G.J., Zou, J.Y., Kjeldgaard, M. & Jones, T.A. Model building and computer graphics. in *International Tables for Crystallography, Vol. F, Crystallography of biological macromolecules* (eds. Rossmann, M.G. & Arnold, E.) 353–356 (Kluwer Academic Publishers, The Netherlands; 2001).
32. Read, R.J. Improved Fourier coefficients for maps using phases from partial structures with errors. *Acta Crystallogr. A* **42**, 140–149 (1986).
33. Brunger, A.T. *et al.* Crystallography & NMR system: a new software suite for macromolecular structure determination. *Acta Crystallogr. D* **54**, 905–921 (1998).
34. Murshodov, G.N., Vagin, A.A., Lebedev, A., Wilson, K.S. & Dodson, E.J. Efficient anisotropic refinement of macromolecular structures using FFT. *Acta Crystallogr. D* **55**, 247–255 (1999).
35. Sheldrick, G.M. & Schneider, T.R. SHELXL: high-resolution refinement. *Methods Enzymol.* **277**, 319–343 (1997).
36. Laskowski, R.A., MacArthur, M.W., Moss, D.S. & Thornton, J.M. PROCHECK — a program to check the stereochemical quality of proteins. *J. Appl. Crystallogr.* **26**, 283–291 (1993).
37. Kraulis, P.J. MOLSCRIPT: a program to produce both detailed and schematic plots of protein structures. *J. Appl. Crystallogr.* **24**, 946–950 (1991).
38. Merritt, E.A. & Murphy, M.E.P. Raster3D version 2.0. A program for photorealistic molecular graphics. *Acta Crystallogr. D* **50**, 869–873 (1994).
39. Esnouf, R.M. Further additions to MolScript version 1.4, including reading and contouring of electron-density maps. *Acta Crystallogr. D* **55**, 938–940 (1999).
40. Sanner, M.F., Spehner, J.-C. & Olson, A.J. Reduced surface: an efficient way to compute molecular surfaces. *Biopolymers* **38**, 305–320 (1996).
41. Bashford, D. An object-oriented programming suite for electrostatic effects in biological molecules. Scientific computing in object-oriented parallel environments. in *Lecture Notes in Computer Science* Vol. 1343 (eds. Ishikawa, Y., Oldehoeft, R.R., Reynders, J.V.W. & Tholburn, M.) 233–240 (Springer, Berlin; 1997).

© 2003 Nature Publishing Group http://www.nature.com/naturestructuralbiology